

## A COMPLETELY NOVEL MECHANISM OF METAL-NONMETAL TRANSITION IN EXPANDED SELENIUM

F. Yonezawa<sup>\*</sup>, H. Ohtani<sup>a</sup>, T. Yamaguchi<sup>b</sup>

Department of Physics, Keio University, 3-14-1 Hiyoshi, Kohokuku,  
Yokohama 223-8522, Japan

<sup>a</sup>National Institute for Fusion Science, 322-6 Oroshi-cho, Toki 509-5292, Japan

<sup>b</sup>Department of Physics, Tokyo Women's University, Tokyo 162-8666, Japan

The purpose of the present article is to review our discovery concerning a completely new mechanism of metal-nonmetal (M-NM) transition in expanded Se. Several mechanisms were previously proposed for M-NM transitions which includes the Bloch-Wilson transition, the Mott-Hubbard transition and the Anderson transition. In each of these cases, a transition takes place from metal to nonmetal when the system is expanded. This behavior is brought about by the narrowing of bands on the increase of volume, which leads to the opening-up of bands and the appearance of an energy gap at the Fermi level. On the other hand, a transition occurs in expanded Se from nonmetal to metal on expansion, which is perfectly against the common knowledge. In expanded Se, chains are fragmented into small sizes of 10, and consequently some of bonds are stretched. We show that the energy splitting  $E_{\tilde{\sigma}^*-\tilde{\sigma}} \equiv E_{\tilde{\sigma}^*} - E_{\tilde{\sigma}}$  corresponding to these stretched bonds becomes smaller, and eventually the gap between the valence band (composed of the lone-pair orbitals) and the conduction band (composed of the anti-bonding  $\tilde{\sigma}^*$  orbitals relevant to the stretched bonds) closes and the system transforms from nonmetal to metal.

(Received July 4, 2005; accepted July 21, 2005)

*Keywords:* Selenium, Metal-nonmetal transition

### 1. Introduction

A metal-nonmetal (M-NM) transition is a macroscopically observable phenomenon of great interest, from which the microscopic behaviors of electronic properties are detected. Several mechanisms for M-NM transitions have been proposed so far, which include (1) the Bloch-Wilson transition, (2) the Mott-Hubbard transition and (3) the Anderson transition. In these M-NM transitions, the relative magnitudes of a characteristic parameter and the width  $W$  of the corresponding bands play deciding roles.

(1) In the case of the Bloch-Wilson transition, the characteristic parameter is the energy difference  $E_{ij} \equiv E_j - E_i$  between the centers  $E_i$  and  $E_j$  of the two relevant bands. Schematic situation of energy bands is presented in Fig. 1(a). Some typical materials in connection with this mechanism are elements in group IIa or IIb such as Hg, for which  $E_{ij} = E_{sp}$ ,  $s$  and  $p$  denoting the  $s$  and  $p$  band, respectively. Liquid Hg just above the melting temperature  $T_m$ , for example, has energy bands as illustrated in the low volume region in Fig. 1(b), where the  $s$  and  $p$  bands overlap and the density of states (DOS) at the Fermi level is finite, thus the system being metallic. When the volume is increased, the band widths ( $W$ ) are narrowed while the difference  $E_{ij}$  remains almost constant. As a result, there appears an energy gap between the  $s$  and  $p$  band as depicted in Fig. 1(b) and the (M  $\rightarrow$  NM) transformation occurs. The increase of volume over a wide range is rather difficult to realize, but can be made possible, for instance, by applying high pressure and high temperature so as

---

\* Corresponding author: yonezawa@xa2.so-net.ne.jp

to bring the system from  $T_m$  to the supercritical region as indicated by an arrow in the pressure-temperature (P - T) plane as shown in Fig. 1(a).

(2) In the case of the Mott-Hubbard transition, the characteristic parameter is the intensity of electron correlation,  $U$ , and an argument analogous to expanded Hg in terms of Figs. 1(a) and (b) applies to this case as well, by using  $U$  instead of  $E_{ij}$  and by employing the lower and upper Hubbard band instead of the s and p band. Liquid alkali metals are practical materials in which the expansion of the system leads to the (M  $\rightarrow$  NM) transition due to electron correlation. (3) In the Anderson transition, the characteristic parameter is the degree of randomness,  $\Gamma$ , which defines the width of the mobility gap.

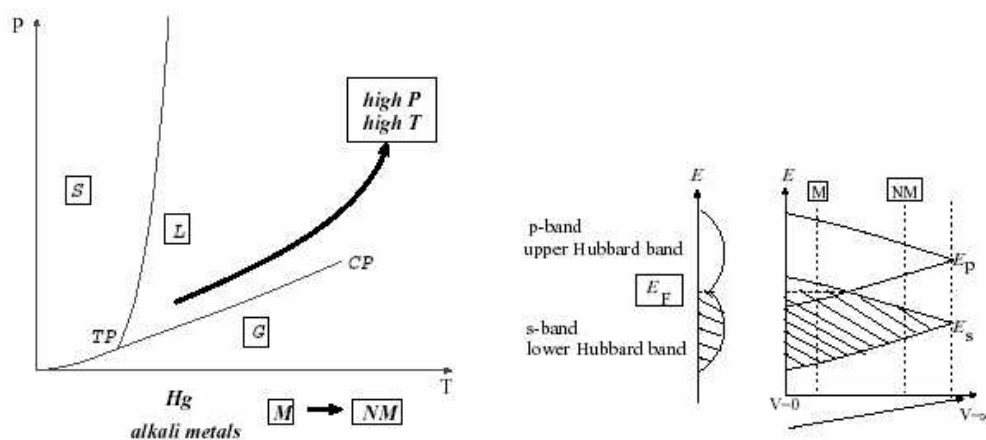


Fig. 1. (a) Schematic illustration of experimental results in the pressure-temperature (P - T) space in the cases of Hg and alkali metals. (b) A schematic explanation of the mechanism for M-NM transitions of the Bloch-Wilson type or the Mott-Hubbard type presented in the volume-energy (v - E) plane. In the Bloch-Wilson mechanism, the two bands are the s- and p-band, while in the Mott - Hubbard mechanism, the two bands are the lower and upper Hubbard band. The levels in the shaded region are occupied.

The details about these three kinds of mechanisms for M-NM transitions are listed in the three corresponding rows in Table 1. As the system is expanded in each of these cases, the band width  $W$  is increased while the magnitude of the respective characteristic parameter is hardly influenced. As a consequence, the ratio  $(W/E_{ij})$ ,  $(W/U)$  or  $(W/\Gamma)$  decreases accompanying the increase of volume  $V$  (or equivalently to the decrease of density) so that the open-up of the bands takes place, and, accordingly the system transforms from a metallic to nonmetallic state. Actually, in all previously known examples, a metal-to-nonmetal (M  $\rightarrow$  NM) transition always takes place when  $V$  is increased.

On the other hand, a nonmetal-to-metal (NM  $\rightarrow$  M) transition is observed experimentally on the increase of  $V$  in expanded liquid selenium (Se) realized under high pressure and high temperature, which is precisely the other way around judging from the common knowledge. Despite some intensive study, this unexpected phenomenon was left unsolved for some time since no traditional ideas worked, but several years ago we discovered a completely novel mechanism for M-NM transitions which successfully elucidated this unprecedented problem about the M-NM transition in expanded Se. The purpose of the present article is to give a fundamental review on this discovery of ours. (All the related information is obtained in refs. [1-11]).

In section 2, experimental results about expanded Se are presented. In section 3, we propose a structural model for expanded Se in 1D and discuss the results of our energy calculations for this model. The essential aspects of our new mechanism for M-NM transitions are found even in our 1D model. In section 4, we present our 3D model and show that the results of energy analyses reinforce the validity of our new mechanism. In section 5 are given discussions and conclusions.

Table 1. Mechanisms for M-NM transitions.

kind of transition	$v \nearrow$	$\Rightarrow$	$W \searrow$	transition as $v \nearrow$
	mechanism	specific quantity	ratio of W & quantity	
Bloch-Wilson	band overlap	$E_{ij} \rightarrow \left(\frac{W}{E_{ij}}\right) \searrow$		M $\Rightarrow$ NM
Mott-Hubbard	Electron correlation	$U \rightarrow \left(\frac{W}{U}\right) \searrow$		
Anderson	disorder	$\Gamma \rightarrow \left(\frac{W}{E_{\Gamma}}\right) \searrow$		
our new transition	energy splitting	$E_{\sigma^*-\sigma} \downarrow \left(\frac{W}{E_{\sigma^*-\sigma}}\right) \nearrow$		NM $\Rightarrow$ M

**2. Experimental results for expanded selenium**

The experiments due to Tamura et al. show that the dc conductivity  $\sigma$  of liquid Se increases by 8 orders of magnitude when the temperature  $T$  is increased along the iso-pressure line as denoted by a rightward arrow in the  $P$ - $T$  plane in Fig. 2(a), while the system is expanded as much as the 20% increase of volume. Note that the horizontal dotted line denotes the critical conductivity which separates a metallic and nonmetallic region. This critical conductivity here is chosen to be Mott’s minimum metallic conductivity  $\sigma_{min}$  for liquids, its value being  $30 \Omega^{-1}cm^{-1}$ . The conductivity beyond  $\sigma_{min}$  is at most a few hundreds in  $\Omega^{-1}cm^{-1}$ , which is comparable with  $\sigma$  of a semimetal. This fact indicates that Se in this metallic phase in the supercritical region is not highly metallic.

As shown in Fig. 2(b), some other physical properties such as the optical absorption and ac conductivity  $\sigma(\omega)$  also lend support to the occurrence of the NM  $\rightarrow$  M transition at the volume (indicated by a vertical broken line) corresponding to  $\sigma_{min}$ . The absorption edge appears at  $T_{NM \rightarrow M}$  and the ac conductivity  $\sigma(\omega)$  changes from semiconductor’s behavior to the Drude behavior characteristic of metallic phases.

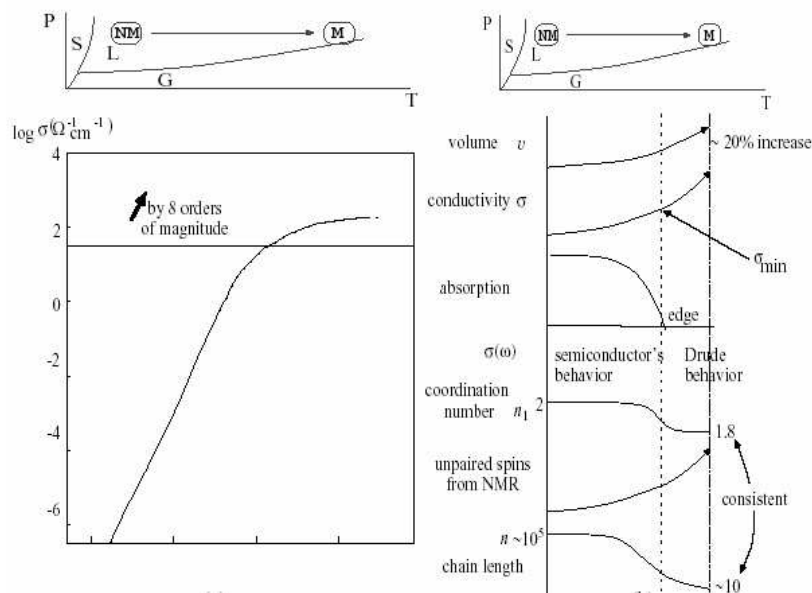


Fig. 2. (a) In the top is shown a schematic illustration in the  $P$ - $T$  space of the iso-pressure line for expanded Se along which the experiments have been carried out, while in the bottom is presented the change of conductivity along the iso-pressure line at  $P = 1400$  bar. The dotted line denotes Mott’s minimum metallic conductivity  $\sigma_{min}$  for liquid metals, which separates metallic and nonmetallic region. (b) The changes of various physical properties in liquid Se from the melting temperature to the temperature region in the vicinity of the critical point.

The atomic structures also have been studied experimentally by means of X-ray diffraction measurements, the X-ray absorption fine structure (XAFS), the extended X-ray absorption fine structure (EXAFS), and the nuclear magnetic resonance (NMR). As demonstrated in Fig. 2(b), the coordination number  $n_1$  decreases from  $n_1 = 2$  typical to a normal chain structure to  $n_1 = 1.8$  which corresponds to the situation that 10 % of the Se bonds are terminated while the underlying chain structure is maintained.

The number of unpaired spins estimated from the measurements of NMR indicates that the chain length  $n$  changes from  $n \sim 10^5$  just above  $T_m$  to  $n \sim 10$  in the supercritical region, which is consistent with the conclusion drawn from the change of the coordination number  $n_1$ .

### 3. Structural model and calculational method

From the experimental results presented in the preceding section, it is expected that supercritical Se is composed of fragmented chains of approximately size 10 distributed randomly as schematically illustrated in Fig. 3. Various kinds of disorder would exist such as disorder in chain size, chain shape, entanglements of chains and chain distributions. Thermal effects also exist. In spite of all these complex aspects, the most essential factor is that the chains are fragmented. By taking this point into account, we construct a structural model as presented in Fig. 4. Our model system is composed of finite chains, each of which has the rotation angle  $\phi = 120^\circ$  as shown in Fig. 4(a). We arrange the finite chains of the same size in a regular manner as presented in Figs. 4(b) and (c), which are the schematic illustration as viewed from the side and top respectively. Although an example of finite chains with size 6 is given in Figs. 4(a) and (b), the chains can be of any size. The bond length is  $r_1$  and the separation between finite chains is  $r_{\text{sep}}$  along the chain axis, while the inter-chain distance is  $a$ . We note here again that the regularity of chain configurations is only for the sake of computational convenience and it does not spoil the generality of our argument because the most important factor is that the chains are fragmented.



Fig. 3. Expected configurations of liquid Se in the vicinity of the critical point.

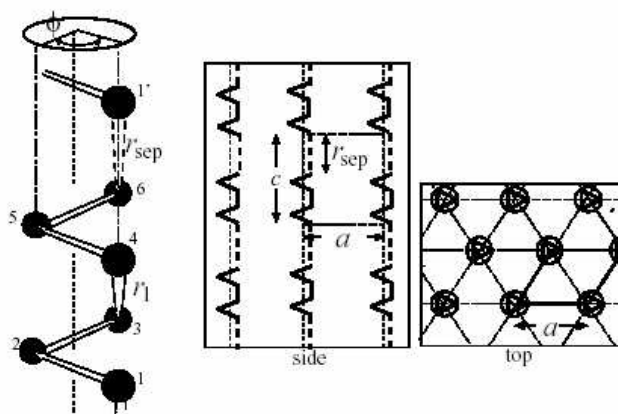


Fig. 4. Our structural model for liquid Se near the critical point; a 3D assembly of fractured Se chains where each fractured chain is of size 6 and  $\phi$  is the rotational angle, which is  $120^\circ$  in the present case. The length of a stretched bond is expressed by  $r_{\text{sep}} > r_1$ , which measures the separation distance between the terminal atoms of two vertically adjacent chains;  $a$  represents inter-chain distance, and  $c$  is the lattice constant. (a) A schematic illustration of vertically aligned chains, (b) and (c) respectively depict the schematic situation when the model structure is viewed from the side and the top.

We calculate both eigenvalues and eigenfunctions. From the knowledge concerning eigenvalues, we can derive band structures, band gaps  $E_g$ , and the band overlap  $E_{\text{overlap}}$ . On the other hand, eigenfunctions are used to obtain the constant-density surfaces of the electron density, which gives an idea about the ways how the wave functions are extended in the real space.

Eigenvalues are calculated in the density functional theory with the local-density approximation, by means of the simulated annealing method, where we perform the norm-conserving pseudopotential due to Bachelet, Hamann and Schlüter. A simulation box is taken to be a primitive cell of hexagonal close-packed structure, and the energy cutoff is chosen to be 10 Ry. In our simulations, periodic boundary conditions are adopted. The size of a simulation box is chosen appropriately for the values of  $r_{\text{sep}}$  and  $a$ .

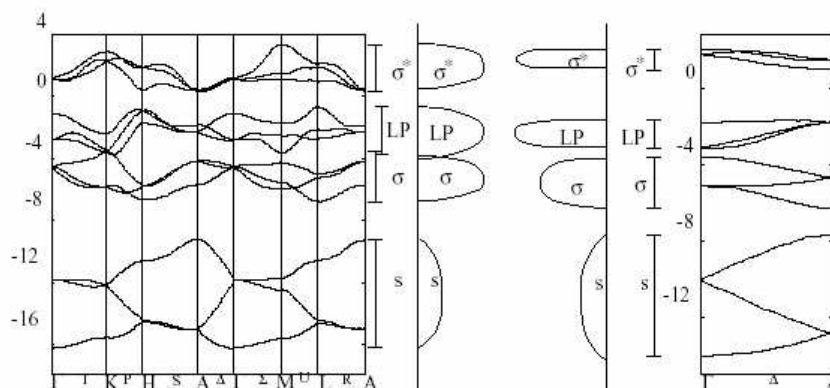


Fig. 5. Band structures and schematic densities of states for 3D crystalline Se (left) with trigonal structure and a 1D crystalline Se of helical chain (right) with 3-fold symmetry.

## 4. Results

### 4.1 Crystalline Se — 1D and 3D

Before studying the results of our energy calculations for general cases, let us first discuss the energy bands for crystalline structures. A three-dimensional (3D) is realized when we take  $r_1/r_0 = r_{\text{sep}}/r_0 = a/a_0 = 1$  in our structural model presented in Fig. 4. Here  $r_0$  and  $a_0$  are respectively the bond length and the inter-chain distance of a crystalline Se with a trigonal structure, which is referred to as trigonal Se (often abbreviated as t-Se).

The band structure is shown on the left of Fig. 5, together with the schematic illustration of the DOS. For comparison's sake, we present on the right of Fig. 5 the band structure and the corresponding DOS for a one-dimensional (1D) crystal of an infinite helical chain with 3-fold symmetry. This 1D crystalline structure is realized by taking  $r_1/r_0 = r_{\text{sep}}/r_0 = 1$  and  $a/a_0 = \infty$  in our structural model explained in Fig. 4.

For both 1D and 3D crystals, the bands are fully occupied up to the lone-pair (LP) bands while the  $\sigma^*$  bands composed of anti-bonding electrons are empty, thus the systems being semiconducting or nonmetallic (NM). The band widths are narrower for the 1D crystal than for the 3D crystal, since the electron wavefunctions for the former case extend only in the 1D space while they extend in the 3D space. Accordingly the energy gap  $E_g$  of about 1.5 eV for t-Se is smaller than  $E_g$  of about 2 eV for 1D crystal. Note that the calculated value of  $E_g \sim 1.5$  eV for t-Se is in fair agreement with the experimental value of  $E_g \sim 1.8$  eV, showing the validity of our calculational method.

### 4.2 Expanded Se — 1D

Now we calculate the energy levels of 1D expanded Se which corresponds to taking  $r_{\text{sep}}/r_1 > 1$  and  $a/a_0 = \infty$  in our structural model. For our energy calculations, we choose size of each fragmented chain to be six. The calculated band energies are demonstrated in Fig. 6. We can see

that, when  $r_{\text{sep}}/r_1$  is increased from unity, one branch out of 6 anti-bonding ( $\sigma^*$ ) bands starts being detached from the other 5 anti-bonding branches and shifting into the energy gap as shown in Fig. 6(b).

This result is explained as follows. As we can see from our structural model in Fig. 4, the increase of  $r_{\text{sep}}/r_1$  indicates that one bond out of 6 bonds in a unit cell is stretched, and consequently the energy splitting  $\Delta E \equiv E_{\tilde{\sigma}^*-\tilde{\sigma}} \equiv E_{\tilde{\sigma}^*} - E_{\tilde{\sigma}}$  between the bonding level  $E_{\tilde{\sigma}}$  and the anti-bonding level  $E_{\tilde{\sigma}^*}$  corresponding to that the stretched bond is decreased. This reduction of the energy splitting causes the downward shifting of the  $\tilde{\sigma}^*$  branch relative to the other bands. Here, we use the notation tilde to describe that any quantity described with a tilde is related to the stretched bond.

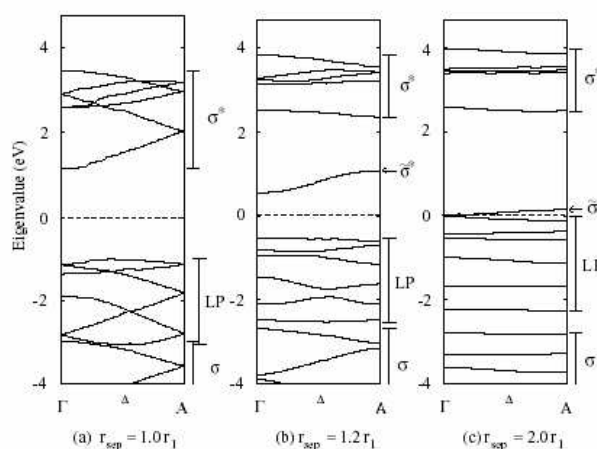


Fig. 6. Band energies for our 1D structural model presented in Fig. 4(a), the results being presented for (a)  $r_{\text{sep}}/r_1 = 1$  (which corresponds to a 1D crystalline Se), (b)  $r_{\text{sep}}/r_1 = 1.2$  and (c)  $r_{\text{sep}}/r_1 = 2.0$ .

When the bond in question is stretched further, the splitting  $E_{\tilde{\sigma}^*-\tilde{\sigma}}$  becomes smaller and the corresponding anti-bonding branch  $\tilde{\sigma}^*$  finally merges with the LP band as shown in Fig. 6(c), which yields the combination of the  $\tilde{\sigma}^*$  levels and the LP levels to be unfulfilled and the system to be metallic.

Concerning the explanation of the M-NM transition in terms of the relative magnitudes of a characteristic parameter and the width  $W$  of the bands, the characteristic parameter is the energy splitting  $E_{\tilde{\sigma}^*-\tilde{\sigma}}$  of the bonding ( $\tilde{\sigma}^*$ ) and anti-bonding ( $\tilde{\sigma}$ ) level. In spite of the fact that the band width  $W$  is decreased on the volume expansion, the decrease of the energy splitting  $E_{\tilde{\sigma}^*-\tilde{\sigma}}$  is so distinguished that the ratio  $W/E_{\tilde{\sigma}^*-\tilde{\sigma}}$  increases as the system is expanded. This is exactly the mechanism of the  $M \rightarrow \text{NM}$  transition in expanded Se, which is a completely new type.

### 4.3 Expanded Se — 3D

The same situation takes place in the band structures of 3D expanded Se as shown in Fig. 7, in which the results for  $(\nu/\nu_0) = 1.3$  and  $1.4$ , where  $\nu$  and  $\nu_0$  are respectively the volume of the extended system and of t-Se. In case of  $(\nu/\nu_0) = 1.3$  (Fig. 7(a)), there exists an energy gap between the highest LP band and the lowest  $\tilde{\sigma}^*$  band, showing that the system is still nonmetallic. In case of  $(\nu/\nu_0) = 1.4$  (Fig. 7(b)), on the other hand, the  $\tilde{\sigma}^*$  band and the LP band are overlapping each other, and accordingly the system is metallic.

The energy regions for bands are presented in Fig. 8 as functions of volume. In the same way as for 1D cases, the band gap decreases as  $(V/V_0)$  increases from unity, and disappears at a critical volume between 1.3 and 1.4. In this way, the mechanism for  $M \rightarrow \text{NM}$  transition experimentally observed in expanded Se under high temperature and high pressure is confirmed to

be the decrease of the energy splitting  $E_{\tilde{\sigma}^*-\tilde{\sigma}}$  as the volume of the system is increased. A remarkable point is that the essential aspect of this mechanism is detected even in 1D systems as explained in Fig. 6.

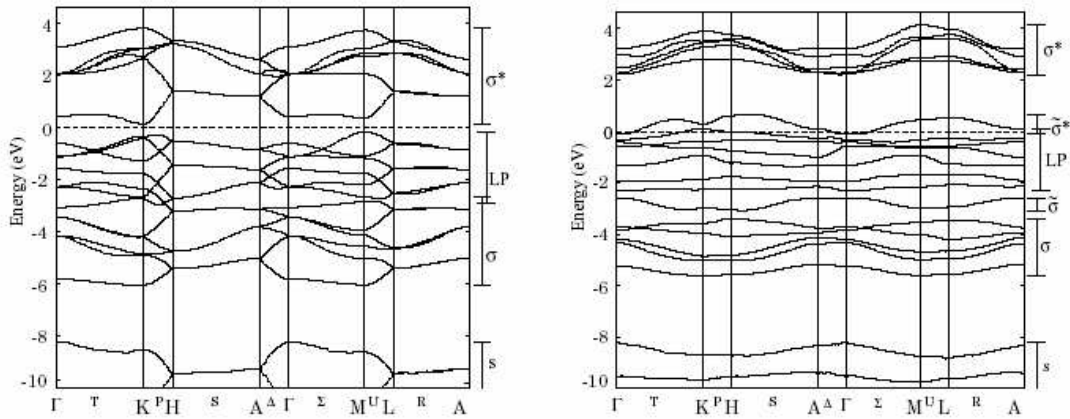


Fig. 7. Band energies for our 3D structural model defined in Fig. 4, the results being shown for, (a)  $(v/v_0) = 1.3$  and (b)  $(v/v_0) = 1.4$ . The dotted line in (a) represents the position of the chemical potential, while the dotted line in (b) corresponds to the Fermi energy.

## 5. Discussion

A remarkable point about liquid Se under high temperature and high pressure is that the expansion of the system can be achieved over a wide range of volume so that both nonmetallic and metallic phase are realized in one material.

If it is possible to find a situation that a practical increase of volume is fulfilled through a group of materials that have the same atomic configurations with different lattice constants. As such an example, we can pick up group IV elements in the periodic table, i.e. C(diamond), Si, Ge and  $\alpha$ -Sn. All of them have a diamond crystalline structure, and the cohesion is covalent via  $sp^3$  hybridized orbitals.

As schematically illustrated by Fig. 9(a) and (b), the valence band (v-band) and the conduction band (c-band) are, respectively, formed of the bonding ( $\sigma$ ) and anti-bonding ( $\sigma^*$ ) band of  $sp^3$  orbitals. The energy gap ( $E_g$ ) is the difference between the bottom level of the c-band ( $\sigma^*$  band) and the top level of the v-band ( $\sigma$  band). As we go down the Periodic Table along group IV elements, the nearest-neighbor inter-atomic  $r_1$  (the length of an  $sp^3$  covalent bond) increases from 1.51 Å for C, through 2.35 Å for Si, and 2.45 Å for Ge, down to 2.81 Å for  $\alpha$ -Sn. This is because, in group IV, the lower an element in the Periodic Table, the bigger the core region and consequently the larger the bond length  $r_1$  becomes.

This situation is as though the same material is uniformly expanded by keeping the diamond structure. The expansion rate from C to  $\alpha$ -Sn is 1.86 times in length and 6.45 times in volume. Since it is practically impossible to expand the volume of a crystal of the same material as much as 6.4 times without causing any transformation in atomic configurations, group IV elements are a very rare and valuable entity concerning which a systematic investigation is possible to elucidate the influence of significant volume change on physical properties.

In relation to our discussion, the change of  $E_g$  is an issue of interest. The band gap  $E_g$  at room temperature is 5.4 eV for V, thus confirming C of the diamond structure as a well-defined insulator;  $E_g$ s for Si and Ge are, respectively 1.17 eV and 0.774 eV, the values characteristic of semiconductors. On the other hand,  $E_g$  is zero for  $\alpha$ -Sn, showing clearly that  $\alpha$ -Sn is a metal.

Fig. 9(b) is drawn on the basis of this information. As in the case of liquid Se, it is clear from Fig. 9(c) that the energy splitting  $E_{\tilde{\sigma}^*-\tilde{\sigma}}$  between the  $\tilde{\sigma}^*$  and  $\tilde{\sigma}$  bands decreases drastically as  $r_1$  increases. From the figures, we observe an M  $\rightarrow$  NM transition of a new type which we have

proposed, or in other words, the band-overlap occurs when the bond length is increased or equivalently when the volume is expanded.

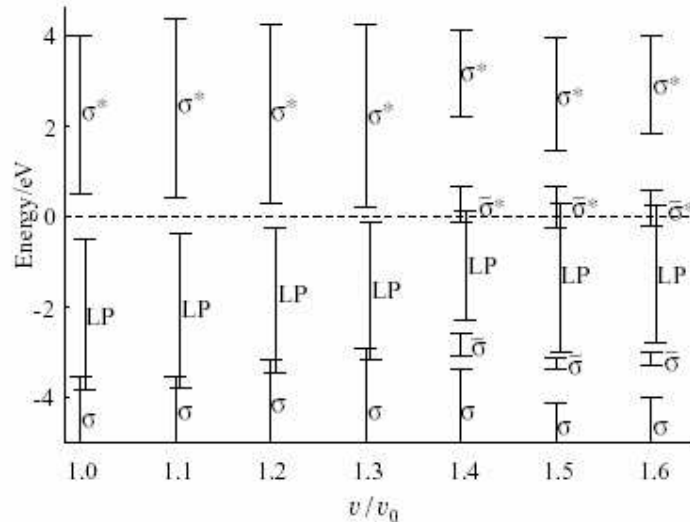


Fig. 8. Energy regions of bands calculated for several values of  $(v/v_0)$ . The horizontal dotted line denotes the position of the chemical potential in the case of nonmetal, or the position of the Fermi level in the case of metal.

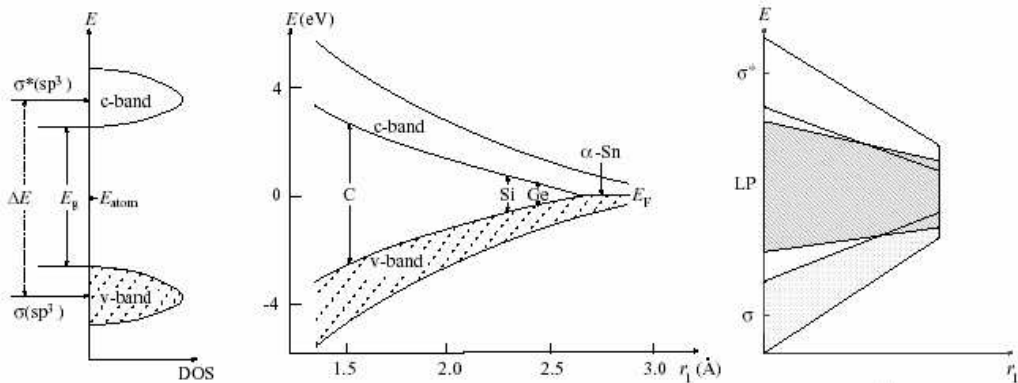


Fig. 9. (a) Schematic illustration of the density of states (DOS) for the valence band (vband) and the conduction band (c-band) in a system with the diamond structure; (b) the relation between the bond length  $r_1$  (the horizontal axis) and the relative positions of the both bands; in comparison with (c) schematic explanation of the bands for our structural model of expanded Se.

## 6. Summary

The results achieved by a series of our works are summarized as follows. We have proposed a completely new mechanism of a transition between metal and nonmetal which explains an unusual behavior of electronic conductivity observed in liquid Se under high temperature and high pressure, being unusual because a transition from nonmetal to metal takes place according to the increase of volume. This behavior is perfectly the other way around when compared to the ordinary mechanisms of metal-nonmetal (M-NM) transitions, in which a transition from metal to nonmetal occurs when the volume is increased.

The key quantity to determine the phenomena of M-NM transition is the ratio of the band width  $W$  and a characteristic parameter specific to each mechanism. As listed in the first three rows of Table 1, the characteristic parameters for usual transitions such as (1) the Bloch-Wilson transition,

(2) the Mott-Hubbard transition and (3) the Anderson transition are respectively (1) the energy difference  $E_{ij} \equiv E_j - E_i$  between the centers  $E_i$  and  $E_j$  of the two relevant bands, (2) the intensity of electron correlation,  $U$ , and (3) the degree of randomness,  $\Gamma$ .

As the volume of the system is increased, the band width  $W$  increases, while these characteristic parameters remain almost fixed. As a consequence, the ratio  $(W/E_{ij})$ ,  $(W/U)$  or  $(W/\Gamma)$  decreases accompanying the increase of volume  $V$  so that the open-up of the bands takes place, and accordingly the system transforms from a metallic to nonmetallic state.

For expanded Se, the characteristic parameter is the energy splitting between the bonding level  $E_{\bar{\sigma}}$  and the anti-bonding level  $E_{\bar{\sigma}^*}$  corresponding to the stretched bond. The volume expansion causes the stretching or weakening of some bonds, which in turn serves to reduce the energy splitting  $E_{\bar{\sigma}^* - \bar{\sigma}} \equiv E_{\bar{\sigma}^*} - E_{\bar{\sigma}}$ . As a result, the gap between the lone-pair band and the anti-bonding ( $\bar{\sigma}^*$ ) band closes and the band-overlap appears. The situation is explained in the last row of Table 1.

## References

- [1] H. Ohtani, T. Yamaguchi, F. Yonezawa, *J. Phys. Soc. Jpn.* **67** (1998) 2807.
- [2] F. Yonezawa, H. Ohtani, T. Yamaguchi, *J. Phys. Condens. Matter* **10**, 11419 (1998).
- [3] F. Yonezawa, H. Ohtani, T. Yamaguchi, F. Yonezawa, K. Tsuji, K. Kaji, M. Doi, T. Fujiwara (Eds.), *The Physics in Complex Liquids*, World Scientific, Singapore, 1998, p.48.
- [4] F. Yonezawa, H. Ohtani, T. Yamaguchi, *J. Non-Cryst. Solids* **250/252**, 510 (1999).
- [5] H. Ohtani, T. Yamaguchi, F. Yonezawa, *J. Non-Cryst. Solids* **250/252**, 428 (1999).
- [6] T. Yamaguchi, H. Ohtani, F. Yonezawa, *J. Non-Cryst. Solids* **250/252**, 437 (1999).
- [7] H. Ohtani, T. Yamaguchi, F. Yonezawa, *Prog.Theor.Phys.Suppl.* **138**, 247 (2000).
- [8] H. Ohtani, T. Yamaguchi, F. Yonezawa, *RIKEN Rev.* **29**, 103 (2000).
- [9] H. Ohtani, T. Yamaguchi, F. Yonezawa, *J. Phys. Soc. Jpn.* **69**, 3885 (2000).
- [10] F. Yonezawa, H. Ohtani, T. Yamaguchi, *J. Non-Cryst. Solids* **293/295**, 199 (2001).
- [11] F. Yonezawa, H. Ohtani, T. Yamaguchi, *Physica B* **296**, 289 (2001).